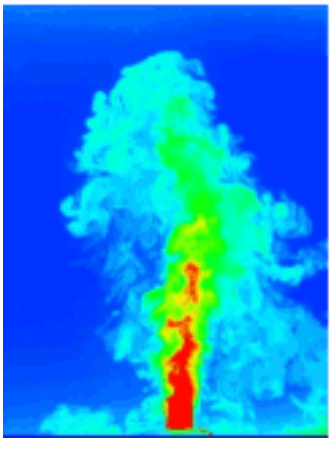

Journal of Turbulence
Publication details, including instructions for authors and subscription information:
http://www.tandfonline.com/loi/tjot20

Intermittent patches of turbulence in a stratified medium with stable shear

Hieu T. Pham [a b], Sutanu Sarkar [a b] & Kraig B. Winters [a b]
[a] Department of Mechanical and Aerospace Engineering, UC San Diego, La Jolla, CA
[b] Scripps Institution of Oceanography, UC San Diego, La Jolla, CA
Published online: 07 Jun 2012.

To cite this article: Hieu T. Pham, Sutanu Sarkar & Kraig B. Winters (2012) Intermittent patches of turbulence in a stratified medium with stable shear, Journal of Turbulence, 13, N20, DOI: 10.1080/14685248.2012.686666

To link to this article: http://dx.doi.org/10.1080/14685248.2012.686666

Journal of Turbulence
Vol. 13, No. 20, 2012, 1–17

Intermittent patches of turbulence in a stratified medium with stable shear

Hieu T. Pham, Sutanu Sarkar* and Kraig B. Winters

Department of Mechanical and Aerospace Engineering, UC San Diego, La Jolla, CA
Scripps Institution of Oceanography, UC San Diego, La Jolla, CA

(*Received 23 January 2012; final version received 14 April 2012*)

Direct numerical simulation (DNS) is used to investigate the evolution of intermittent patches of turbulence in a background flow with the gradient Richardson number, Ri_g, larger than the critical value of 0.25. The base flow consists of an unstable stratified shear layer ($Ri_g < 0.25$) located on top of a stable shear layer ($Ri_g > 0.25$), whose shear and stratification are varied. The unstable shear layer undergoes a Kelvin–Helmholtz shear instability that develops into billows. Vortices associated with the billows are pulled into the bottom shear layer and stretched by the local shear into a horseshoe configuration. The breakdown of the horseshoe vortices generates localized patches of turbulence. Three cases with different levels of shear and stratification, but with the *same* Ri_g, in the bottom shear layer are simulated to examine the popular hypothesis that mixing is determined by local Ri_g. In the case with largest shear and stratification, the vortices are less likely to penetrate the bottom layer and are quickly dissipated due to the strong stratification. In the case with moderate shear and stratification, vortices penetrate across the bottom layer and generate turbulence patches with intense dissipation rate. The case with the mildest level of shear and stratification shows the largest net turbulent mixing integrated over the bottom layer. Analysis of the turbulent kinetic energy budget indicates that the mean kinetic energy in the bottom layer contributes a large amount of energy to the turbulent mixing. In all cases, the mixing efficiency is elevated during the penetration of the vortices and has a value of approximately 0.35 when the turbulence in the patches decays.

Keywords: stratified shear layer; turbulence; vortices

1. Introduction

Shear instability is an important turbulence-generating processes in many environmental flows and the understanding of associated heat and momentum fluxes is of fundamental interest. Previous works have shown that a stratified shear layer with a gradient Richardson number, Ri_g, less than 0.25 somewhere in the layer can develop a shear instability. Here, Ri_g is the ratio of a squared shear rate S^2 to a squared buoyancy frequency N^2. Subsequent nonlinear evolution, such as the formation and the breakdown of Kelvin–Helmholtz (KH) billows, results in turbulence in the vicinity of the shear layer. Recent studies [1,2] indicate that turbulence can be found in regions with $Ri_g > 0.25$, where other flow conditions such as large-scale kinetic energy and local shear rate can play an important role in turbulent mixing. In the present study, we use direct numerical simulations (DNS) to investigate how

*Corresponding author. Email: ssarkar@ucsd.edu

ISSN: 1468-5248 online only

http://dx.doi.org/10.1080/14685248.2012.686666
http://www.tandfonline.com

turbulence characteristics in a stratified shear layer with $Ri_g > 0.25$ depend on different flow conditions.

Linear shear stability theory predicts that a critical value of $Ri_g < 0.25$ somewhere in a flow is a necessary condition for an instability [3]. Although there are discussions, using field data [4, 5] and laboratory experiments [6], of a shear instability at a larger value, the reported Ri_g is often averaged over a time span larger than that of a shear instability. In the present study, we target turbulence found in a stratified shear layer that is linearly stable by the stability theory. Turbulence as a result of the breakdown of KH billows in a stratified shear layer with local $Ri_g < 0.25$ has been studied using laboratory experiments [6–8] and numerical simulations [9–12]. The associated mixing efficiency, defined as a ratio of the dissipation rate of turbulent potential energy, ε_ρ, to that of turbulent kinetic energy (TKE), ε, is found to be significantly larger than 1.0 during the development of the KH billows and has a value in the range of 0.3–0.6 during the decay of turbulence, which is significantly larger than the value of 0.2 used in many ocean models. In a study of the interaction between an unstable shear layer ($Ri_g < 0.25$) and a stable jet ($Ri_g > 0.25$), Pham and Sarkar [2] reported turbulence patches in the jet. Horseshoe vortices associated with KH billows in the shear layer can penetrate the jet and generate turbulence there. The horseshoe vortices are shown to interact with the jet by extracting its mean kinetic energy and dispensing the energy to turbulent mixing. The mixing efficiency in the turbulent patches inside the jet is found to be as large as the value in an unstable shear layer.

The work of Pham and Sarkar [2] has shown that although the local $Ri_g > 0.25$, its mean kinetic energy can still be tapped for turbulence, and therefore, any variations in the background flow can alter its turbulence characteristics. In this investigation, we aim to look at: (1) How do variations in the background shear and stratification affect the turbulence triggering process, i.e., the horseshoe vortex penetration? (2) How do turbulent statistics and mixing differ as the vortices interact with different shear rates and stratification levels? Answers to these questions will help determine if specific details, beyond local Ri_g, about a flow are crucial to the mixing process.

2. Methods

Different from Pham and Sarkar [2], we consider the interaction between two adjacent stratified shear layers in a temporal-evolving frame. One of the shear layers is unstable and located above a stable layer with shear. Initial background flow conditions are homogeneous in streamwise (x) and spanwise (y) directions and vary in the vertical direction (z) in which gravity acts. The initial streamwise velocity profiles shown in Figure 1(a) are constructed by:

$$\langle u_0^* \rangle = \frac{-\Delta U^*}{2} \tanh\left(\frac{z^*}{0.5\delta_{\omega,0}^*}\right) + S_d \Delta U^* \tanh\left(\frac{z^* + 3.5\delta_{\omega,0}^*}{\delta_{\omega,0}^*}\right),$$

where the brackets $< \cdot >$ indicate a horizontal x–y average, superscript $*$ denotes dimensional quantities, and subscript 0 denotes initial values at time $t^* = 0$. ΔU^* is the velocity difference across the top unstable shear layer centered at $z^* = 0$ and $\delta_{\omega,0}^*$ is its initial thickness. The bottom stable shear layer centered at $z^* = -3.5\delta_{\omega,0}^*$ has a thickness of $2\delta_{\omega,0}^*$ and a shear rate of S_d^* at its center. With the velocity in the top shear layer kept constant, three cases with different values of S_d^* in the bottom shear layer are considered in this study. The profiles of the shear rate S are shown in Figure 1(b).

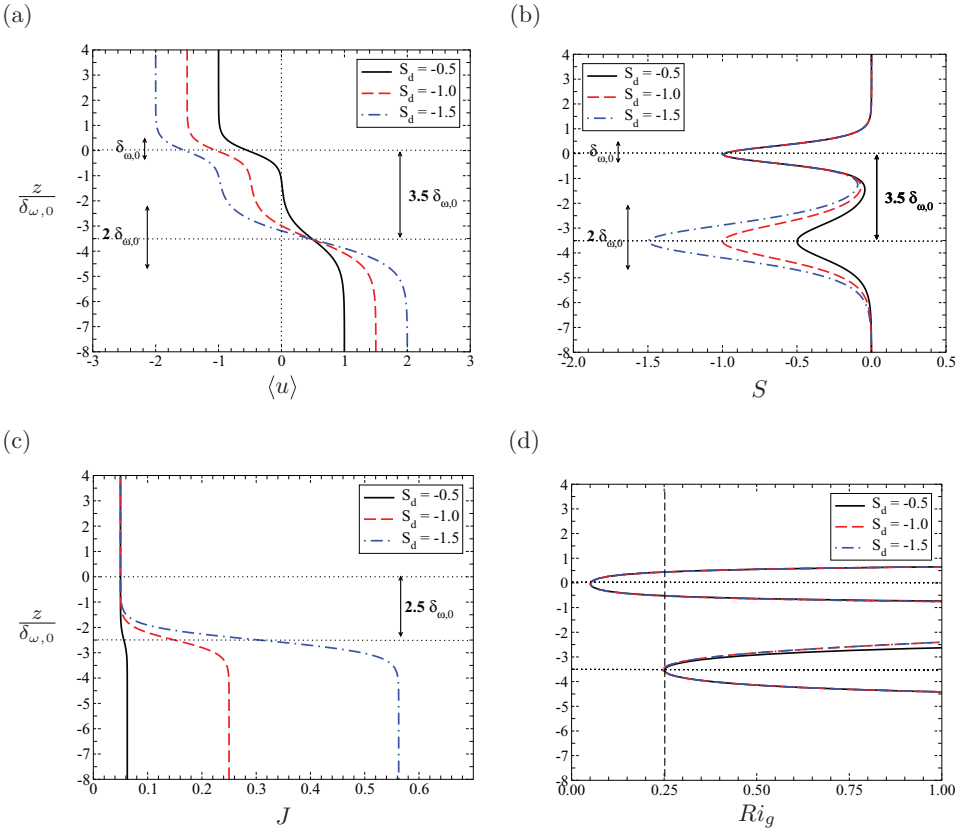

Figure 1. (a) Schematics of *initial* mean streamwise velocity $< u >$, (b) shear rate S, (c) nondimensional Richardson number J, and (d) gradient Richardson number Ri_g. The dashed vertical line in (d) indicates marginal value for shear instability $Ri_g = 0.25$.

Each of the shear layers is linearly stratified in the vertical direction, with the density gradient in the top shear layer weaker than that in the bottom shear layer. The background density has the following stratification profile:

$$J(z) = \frac{J_t + J_b}{2} + \frac{J_t - J_b}{2} \tanh\left(\frac{z^* + 2.5\delta^*_{\omega,0}}{0.5\delta^*_{\omega,0}}\right).$$

Here, $J(z) = N(z)^{*2}\delta^{*2}_{\omega,0}/\Delta U^{*2}$ is the nondimensional Richardson number with the squared buoyancy frequency $N^{*2} = -(g^*/\rho^*_0)d < \rho^* > /dz^*$. The J profiles shown in Figure 1(c) have J_t equal to 0.05 in the top shear layer for all cases. In the bottom shear layer, J is varied with different values of $J_b = 0.0625$, 0.25, and 0.5625 such that the gradient Richardson number Ri_g at the center of the bottom shear layer $z = -3.5$ is equal to 0.25 in all cases. Linear stability analysis of the profiles in Figure 1 indicates that a KH shear instability develops in all cases, with the eigenfunction of streamwise velocity u concentrated in the top shear layer. Nevertheless, according to Pham and Sarkar [2], horseshoe vortices associated with the nonlinear evolution of the KH instability in the top shear layer are able

to penetrate the bottom shear layer and generate turbulence there. In the present study, we will examine the interaction between the horseshoe vortices and the bottom stratified shear layer in different background configurations but with the same Ri_g.

The incompressible Navier–Stokes equations with the Boussinesq approximation are solved in Cartesian coordinates with dependent variables: velocity u, v, w, pressure p, and density ρ; and independent variables: x, y, z, and t. Using $\delta^*_{\omega,0}$, ΔU^*, and $\delta^*_{\omega,0} d < \rho^* > /dz^*|_{-\infty}$ as the characteristic length, velocity, and density, respectively, the nondimensional governing equations take the following form:

$$\nabla \cdot \mathbf{u} = 0, \tag{1}$$

$$\frac{\partial \mathbf{u}}{\partial t} + (\mathbf{u} \cdot \nabla)\,\mathbf{u} = -\nabla p + \frac{1}{Re_0}\nabla^2 \mathbf{u} - J_b \rho' \delta_{i3}, \tag{2}$$

$$\frac{\partial \rho}{\partial t} + (\mathbf{u} \cdot \nabla)\,\rho = \frac{1}{Re_0 Pr}\nabla^2 \rho, \tag{3}$$

where

$$Re_0 = \frac{\Delta U^* \delta^*_{\omega,0}}{\nu^*}, \quad J_b = \frac{N_b^{*2} \delta^{*2}_{\omega,0}}{\Delta U^{*2}}, \quad \mathrm{Pr} = \frac{\nu^*}{\kappa^*}. \tag{4}$$

Here, ν^* and κ^* are the kinematic viscosity and molecular diffusivity, respectively. In all cases, Re_0 and Pr are equal to 1000 and 1, respectively. Hereafter, all quantities are discussed in nondimensional form.

A second-order finite difference method on a staggered grid is used for spatial discretization and the simulation is marched in time with a third-order low-storage Runge–Kutta scheme. The domain size is $50.4 \times 33.6 \times 42.7$ and the grid has $384 \times 256 \times 320$ points in the x-, y-, and z- direction, respectively. Domain decomposition with MPI (message-passing interface) is utilized. The grid is uniform is the streamwise (x) and spanwise (y) directions, with a spacing of 0.13. In the vertical direction, the grid is uniform in the region $-6 < z < 3.75$, with a spacing of 0.075, while it is stretched at the rate of 2% outside. Low-amplitude velocity perturbations with a broadband spectrum,

$$E(k) \propto \left(\frac{k}{k_0}\right)^4 \exp\left[-2\left(\frac{k}{k_0}\right)^2\right],$$

are added to initialize the flow. Here, k_0 is set such that the spectrum peaks at 1.7. Fluctuations are introduced only in the shear layer with the shape function,

$$A(z) = \exp(-z^2),$$

and with a maximum amplitude of 0.1% (ΔU).

Periodic boundary conditions are used in the streamwise and spanwise directions. The top and bottom faces of the domain have the following conditions:

$$
\begin{aligned}
u\left(z_{\min}\right) &= \langle u_0 \rangle \left(z_{\min}\right), \\
u\left(z_{\max}\right) &= \langle u_0 \rangle \left(z_{\max}\right), \\
v\left(z_{\min}\right) &= v\left(z_{\max}\right) = 0, \\
p\left(z_{\min}\right) &= p\left(z_{\max}\right) = 0, \\
\frac{\partial w}{\partial z}\left(z_{\min}\right) &= \frac{\partial w}{\partial z}\left(z_{\max}\right) = 0, \\
\frac{\partial \rho}{\partial z}\left(z_{\max}\right) &= -J_t, \\
\frac{\partial \rho}{\partial z}\left(z_{\min}\right) &= -J_b.
\end{aligned}
$$

A sponge region is constructed at the top ($z > 10$) and the bottom ($z < -20$) boundaries in which the velocity and density are damped toward their initial values at the boundaries. More details about the numerical methods can be found in [13, 14].

3. Visualizations of the turbulent patches

The linear growth of KH shear instability, the nonlinear development of KH billows, and the transition of KH shear instability to turbulence in the top shear layer have been demonstrated in many previous studies [10, 12, 15, 16]. In this study, we only focus on interaction between the horseshoe vortices and the bottom shear layer. Visualizations of the density fields are provided in this section to show the presence of localized patches of turbulence in the region with $Ri_g > 0.25$.

Vertical x–z slices of the density field at $y = 16.7$ in the case with bottom shear of $S_d = -0.5$ are shown in Figure 2(a)–(c) at times $t = 100$, 150, and 200, respectively. At $t = 100$, KH billows roll up in the top shear layer at $z = 0$, with the isopycnals overturned. In the bottom shear layer centered at $z = -3.5$, the isopycnals are flat. At $t = 150$, the billows break down and the top shear layer transitions to turbulence. At the base of the top shear layer, $z = -2$ and $x = 40$, an isopycnal overturn with size smaller than that of the KH billows begins to leave the top shear layer and penetrate the bottom shear layer. This overturn is driven by localized spanwise vortex tubes formed during the breakdown of the KH billows. These tubes are pulled by and interact with the background spanwise vorticity provided by the shear in the bottom layer. At $t = 200$, a large vertical isopycnal displacement is observed in the region $36 < x < 45$ and $-5 < z < -2.5$. The displacement has amplitude as large as the vertical extent of the KH billows in the top shear layer. The isopycnal fluctuations in the bottom shear layer are spatially localized, while they are horizontally widely spread in the top shear layer. From $x = 36$ to $x = 41$, the isopycnal at $z = -2.5$ is displaced downward to $z = -5$ due to the penetration of the vortex tubes into the bottom shear layer. From $x = 41$ to $x = 43$, the isopycnal at $z = -5$ is displaced upward and is overturned. It is important to emphasize that this overturn contributes significantly to local turbulent mixing, besides the downward fluxes associated with the descending vortex tubes.

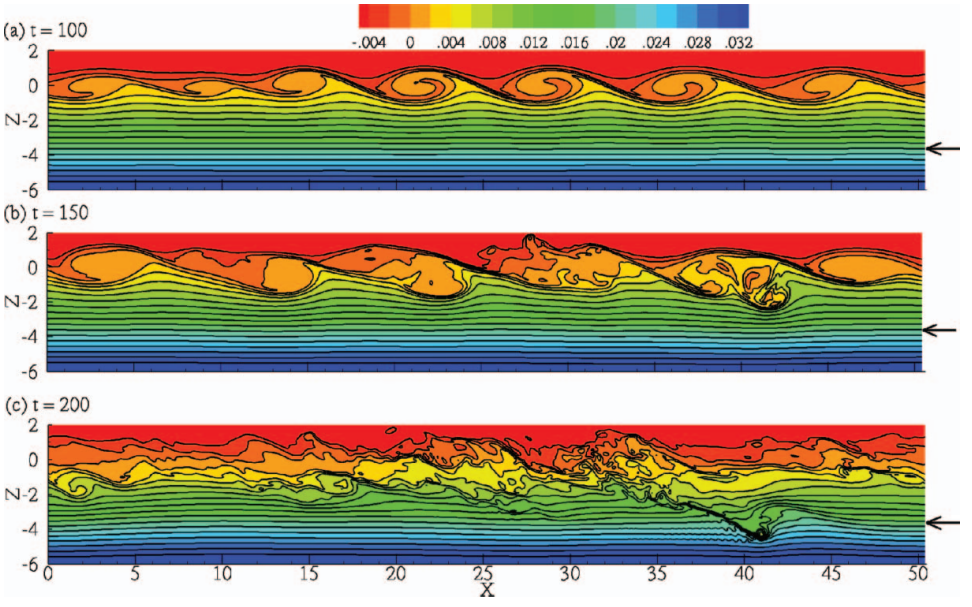

Figure 2. Case $S_d = -0.5$: $x - z$ slices at $y = -16.7$ of the density fields at three times. Arrows indicate the center of the bottom shear layer.

Figure 3(a) provides a 3D view of the density field at $t = 200$ in Case $S_d = -0.5$. It is noted that the figure is flipped upward to ease visualization. The red isosurface depicts isopycnal fluctuations in the top shear layer at $z = 0$. The fluctuations are broadband and homogeneously spread in the horizontal direction. The green isosurface shows fluctuations in the bottom shear layers at $z = -3.5$. The fluctuations at this depth are localized and clustered into patches. It is noted that Figure 2(c) only shows one vertical slice of the domain at $y = 16.7$, and therefore, depicts only one event of a descending vortex. In fact, Figure 3(a) shows multiple distortions of the isopycnal corresponding to several descending vortices that occur at the same time but at different horizontal locations. In Figure 3(b), the red isosurface depicts the 3D structure of the vortices using the λ_2 criterion, which locates the pressure minimum in a plane perpendicular to the vortex axis and accurately defines vortex cores [17]. Comparing Figure 3(a) to Figure 3(b), it is certain that the patches of density fluctuations in the bottom shear layer are triggered by the penetrations of horseshoe vortices. The vortices, which originate as spanwise vortex tubes in the top shear layer, are drawn in and stretched into a horseshoe configuration by the background shear of the bottom layer. In the study of Pham and Sarkar [2], one horseshoe vortex is observed in the spanwise y-direction. In this study, we increase the spanwise domain length twice as large and two vortices can occur at a fixed x-location, e.g., at $x = 2$ in Figure 3(b). The spanwise domain length is significantly larger than two spanwise lengths of the vortices, so it is unclear if the vortex dimension is related to a spanwise instability of the KH shear instability in the top shear layer. During the nonlinear evolution of a KH shear instability, large vortices associated with KH billows break down into smaller vortices. Pham and Sarkar [2] observed that the vortices associated with the KH billows penetrate downward into the jet below. In the present study with a larger spanwise domain, the large vortices break down and only the smaller vortices are observed to penetrate the bottom shear layer.

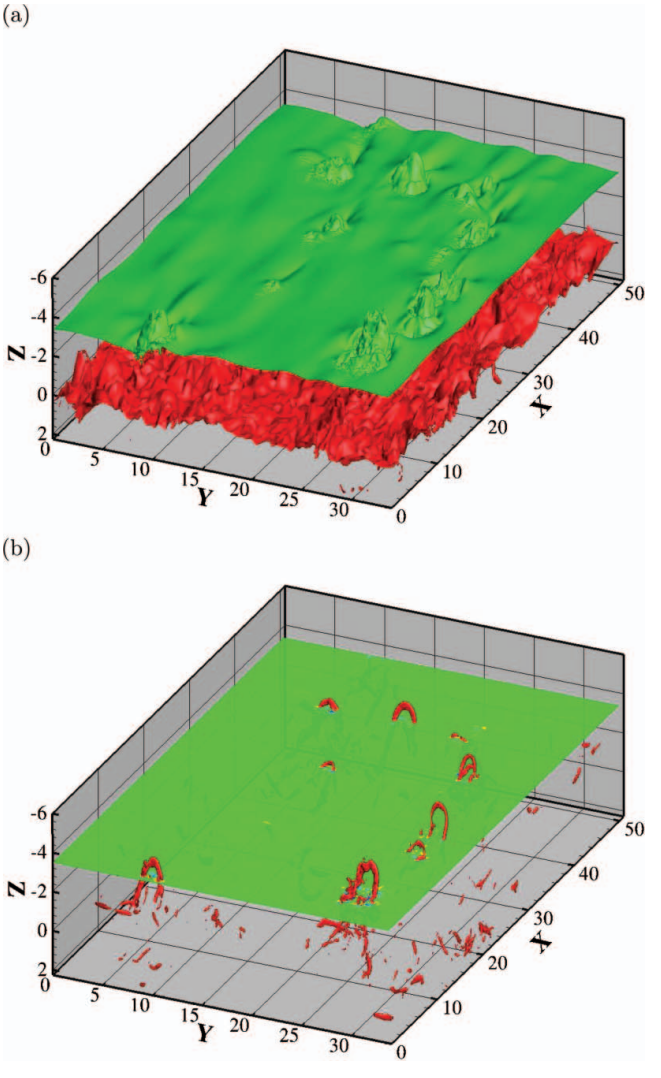

Figure 3. Case $S_d = -0.5$: (a) Isosurfaces of the density field at $t = 200$: $\rho = 0$ (red); $\rho = 0.019$ (green). The red isosurface shows horizontally homogeneous broadband turbulence at $z = 0$, while the green isosurface indicates localized patches of turbulence at $z = -3.5$. (b) Isosurface (red) of $\lambda_2 = -15$ illustrates the horseshoe vortices, which originate from the unstable shear layer at $z = 0$, penetrate, and generate turbulence across the stable shear layer. The horizontal plane shows contours of λ_2 at depth $z = -3.5$. The figure is flipped such that negative z-axis is upward.

Regardless of how a spanwise vortex forms in the top shear layer, if it meanders in close proximity to the bottom shear layer, it is likely to be pulled by the vorticity in the layer. Therefore, a larger shear rate supports stronger attraction and stretching of the vortex. In contrast, a larger density stratification opposes the penetration since the vortex needs to overcome a larger potential energy difference. Figure 4(a)–(c) compares the density fluctuations among the three cases, each at $t = 180$. In Case $S_d = -0.5$, the vortex penetration is observed at $x = 36$ and $z = -3$. At later time, $t = 200$, as shown in

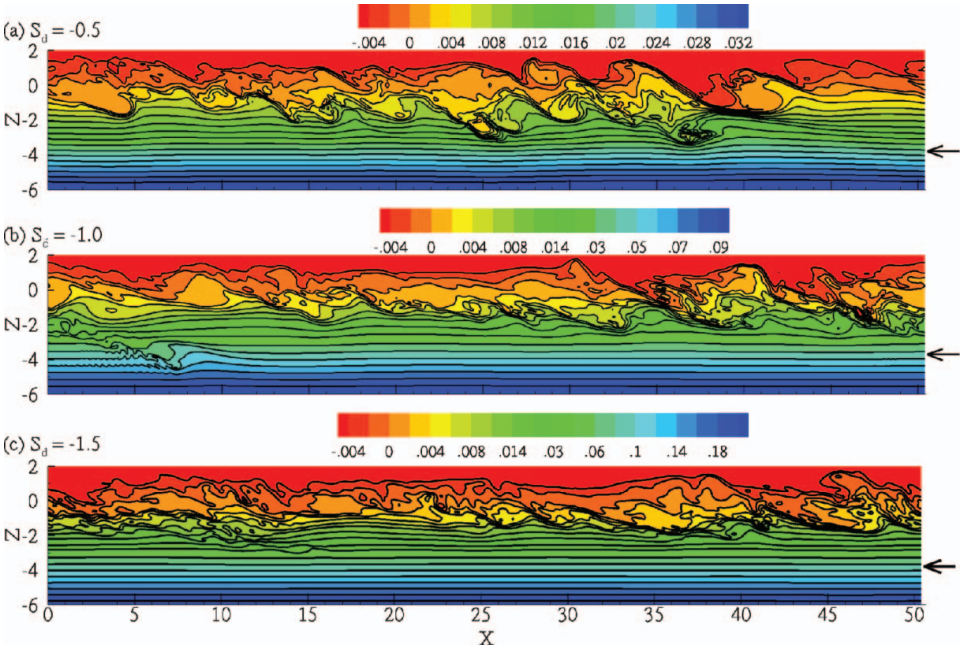

Figure 4. Density fields in $x - z$ slices at $y = -16.7$ in the three cases at $t = 180$. Arrows indicate the center of the bottom shear layer.

Figure 2(c), the vortex is advected rightward and downward to $z = -5$. In Case $S_d = -1.0$, the patch of the density fluctuation is present in the region $0 < x < 10$ and the penetration depth is down to depth $z = -5$. The vortex is least energetic in Case $S_d = -1.5$ since the stratification is strongest in this case. The penetration depth is shallow, with patches of fluctuations observed in the region $9 < x < 15$ and limited to the region above -3. Overall, the vortices in the case with the weakest shear and stratification penetrate to the greatest depth and persist for the longest duration. In Case $S_d = -0.5$, vortices are observed as late as $t = 200$, at which time they are already dissipated in the other two cases. In the case with the strongest shear and stratification, the vortices cannot penetrate as deep and are quickly dissipated. The vortices in the case with medium shear ($S_d = -1.0$) generate the most energetic bursts of turbulence with the strongest dissipation rate, as will be discussed in Sections 5 and 6.

4. Evolution of mean flows

The evolution of KH shear instability in the top shear layer significantly alters the mean quantities there. Momentum and energy are extracted from the mean shear and transferred into turbulence. The shear rate at $z = 0$ decreases in time due to the energy extraction. The stratification there also decreases due to mixing. These observations agree well with previous studies [10, 18]. In contrast, the mean flow conditions in the bottom shear layer vary little in time despite the vortex penetration and the density fluctuations discussed in the last section. Figure 5(a) shows the time evolution of the shear rate S at depth $z = -3.5$, normalized by its initial value S_0. Prior to $t = 150$, the shear decreases in all cases due to viscous effects. As the vortices reach this depth, the shear slightly increases in Case

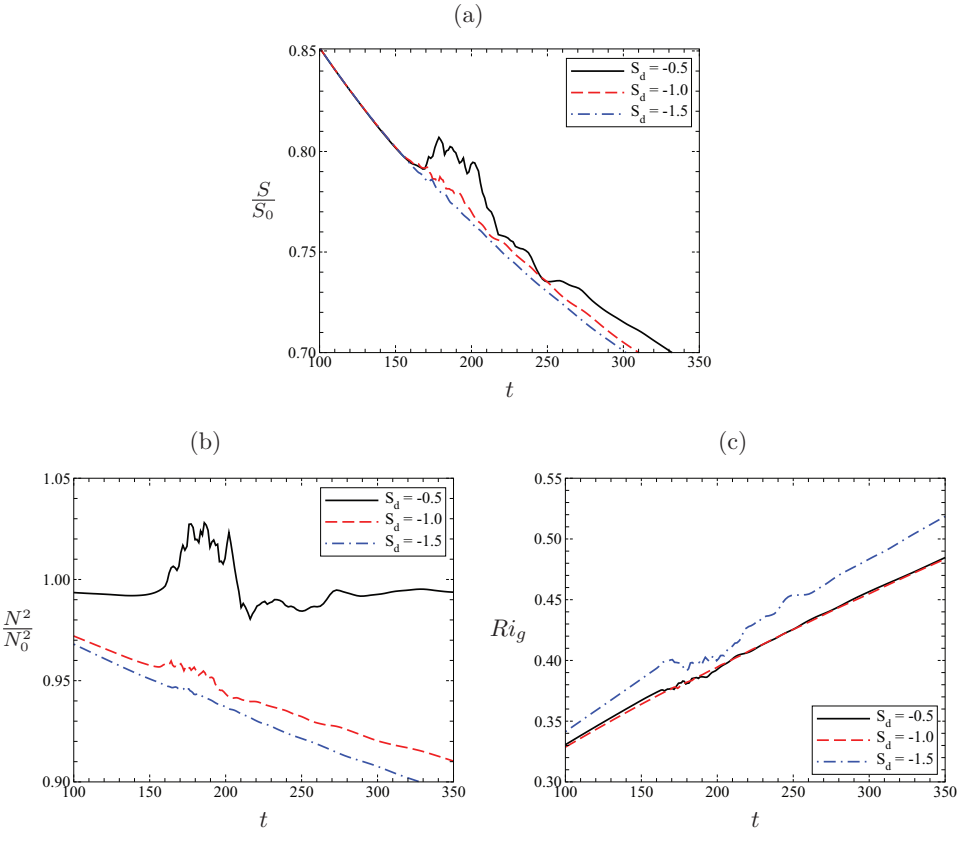

Figure 5. Evolution of mean conditions at depth $z = -3.5$: (a) shear rate and (b) squared buoyancy frequency, both normalized by the corresponding initial values at the same depth; (c) gradient Richardson number.

$S_d = -0.5$, while the variations are minimal in the other two cases. Similar trends are observed in the stratification, as shown in Figure 5(b). The squared buoyancy frequency N^2 in Case $S_d = -0.5$ increases between $t = 150$ and $t = 200$, during which the vortices penetrate the region. The vortices eject light fluid from the top shear layer down into the strongly stratified bottom region, and therefore, steepen the density gradient locally. The squared buoyancy frequency shows a slight increase at $t = 150$ in Case $S_d = -1.0$, while the elevation is not observed in Case $S_d = -1.5$. Over the simulated time, the stratification in these two cases decreases due to molecular diffusion. The gradient Richardson number is shown in Figure 5(c). During the time period $150 < t < 200$, the values of Ri_g are larger than 0.35, *significantly larger* than the critical value 0.25 for a linear shear instability.

It is important to emphasize that the mean quantities discussed here are the values averaged over the entire horizontal domain. Since the size of the vortices is significantly small with respect to the horizontal domain and the patches of density fluctuations are localized, the local values differ greatly from the mean value. For example, the local gradient Richardson number in the bottom shear layer can be less than 0.25, or even negative in regions with positive density gradient, as shown in Figure 4. While the mean Ri_g can be used as an indicator of shear-driven turbulence in the top shear layer, it is not an appropriate

metric for characterizing the intermittent turbulence in the bottom shear layer. The present simulations clearly demonstrate that the turbulence in the top shear layer is driven by the KH shear instability and that in the bottom layer is triggered by the penetration of vortices. While both layers have shear and stratification, linear stability theory is not able to account for the turbulence in the bottom layer.

5. TKE budgets

In this section, the turbulent kinetic budget (TKE) is examined to demonstrate how the background conditions in the bottom shear layer influence the intermittent turbulence. The TKE budget for the simulated flows is described by the following equation:

$$\frac{dK}{dt} = P - \varepsilon + B - \frac{dT_3}{dz}, \tag{5}$$

where, $K = 1/2 < u_i' u_i' >$ is the TKE, P is the production rate, defined as

$$P = -\left\langle u'w' \right\rangle \frac{d\left\langle u \right\rangle}{dz},$$

ε is the dissipation rate,

$$\varepsilon \equiv \frac{2}{Re_0} \left\langle s_{ij}' s_{ij}' \right\rangle ; s_{ij}' = \frac{1}{2} \left(\frac{\partial u_i'}{\partial x_j} + \frac{\partial u_j'}{\partial x_i} \right),$$

and B is the buoyancy flux, defined as

$$B = -J_b \left\langle \rho' w' \right\rangle .$$

The transport term dT_3/dz is defined as

$$T_3 = \frac{1}{2} \left[\left\langle w'u'u' \right\rangle + \left\langle w'v'v' \right\rangle + \left\langle w'w'w' \right\rangle \right] + \frac{\left\langle p'w' \right\rangle}{\rho_0} - \frac{2}{Re_0} \left[\left\langle u's_{31}' \right\rangle + \left\langle v's_{32}' \right\rangle + \left\langle w's_{33}' \right\rangle \right].$$

In Equation (5), the apostrophe indicates fluctuating quantities within the framework of Reynolds decomposition. In the present study, which involves a continuously stratified background density, TKE can be transported by internal waves and turbulence. The dynamics of internal waves excited by a KH shear instability has been discussed at length in previous literature [2, 18]. Here, we focus on the turbulent transport associated with the penetration of the vortices.

Figure 6(a)–(c) plots the dissipation fields corresponding to the density fields shown in Figure 4. The dissipation rate inside the patches of density fluctuations in the bottom shear layer is comparable to the value in the top shear layer. Therefore, the turbulence triggered by the vortex penetrations is not negligible even though it is localized and intermittent. The patches of dissipation with values greater than 10^{-3}, shown in red in the bottom shear layer, are larger in size and impinge to a greater depth in Cases $S_d = -0.5$ and -1.0 compared with Case $S_d = -1.5$. In the latter case, the vortices are quickly broken down by the strong stratification. It is noted that in Case $S_d = -0.5$, the red patch at $x = 36$ and $z = -3$ in Figure 6(a) continues to deepen and reach $z = -5$ at $t = 200$, as shown in Figure 2(c). At this late time, the vortices in the other two cases have been dissipated.

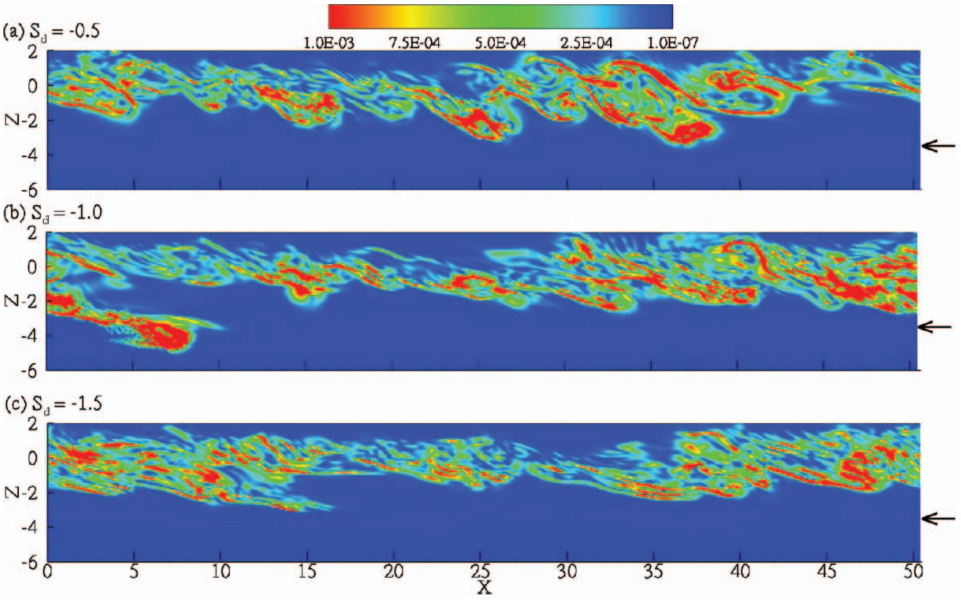

Figure 6. Dissipation fields in $x-z$ slices at $y=-16.7$ in the three cases at $t=180$. Arrows indicate the center of the bottom shear layer.

The TKE budgets at $t=150$ before the vortex penetration are shown in Figure 7(a), (c), and (e) and those at $t=180$ during the penetration are plotted in Figure 7(b), (d), and (f) for the three cases. Prior to the vortex penetration, the budgets are similar among the cases, with the production and dissipation concentrated in the top shear layer. At $z=-2$ between the top and the bottom shear layer, the transient term dK/dt is balanced by the transport term dT_3/dz. TKE is extracted from the center of the top shear layer at $z=0$ and is transferred downward via pressure (wave) and turbulent transport. At $t=180$, significant production and dissipation are observed inside the bottom shear layer. In Case $S_d=-0.5$ shown in Figure 7(b), at $z=-4$, the positive transient term is balanced by the downward turbulent transport associated with the penetration of the vortices. The production increases due to the interaction of the transported turbulence with the background shear. The dissipation is not yet elevated, although at later time, when the penetrating vortex breaks down, the dissipation is higher at this depth. In Case $S_d=-1.0$ shown in Figure 7(d), the profiles in the budget spread down to $z=-5$. At this time, the vortices have broken down so that the profiles of the transient and transport terms in the bottom shear layer change signs rapidly in the vertical direction. The budget in Case $S_d=-1.5$ shown in Figure 7(f) does not spread as deep. The production and dissipation in the bottom shear layer are significantly smaller than the values observed in other cases.

To illustrate the time evolution of the TKE budget, we plot the budgets at depth $z=-3.5$ as a function of time in Figure 8(a)–(c). Prior to the penetration, the terms in the budgets are not zero due to the activity of internal waves propagating across the bottom shear layer; however, the energetic effects due to waves are small relative to the effects of vortex penetrations [2]. When the vortices penetrate the center of the bottom shear layer $z=-3.5$, the transport term exhibits sudden bursts of downward energy transport, resulting in a gain in TKE (positive dK/dt). It is important to emphasize that these bursts in the transport term are attributed to turbulence transport (the triple velocity correlation in the definition of T_3),

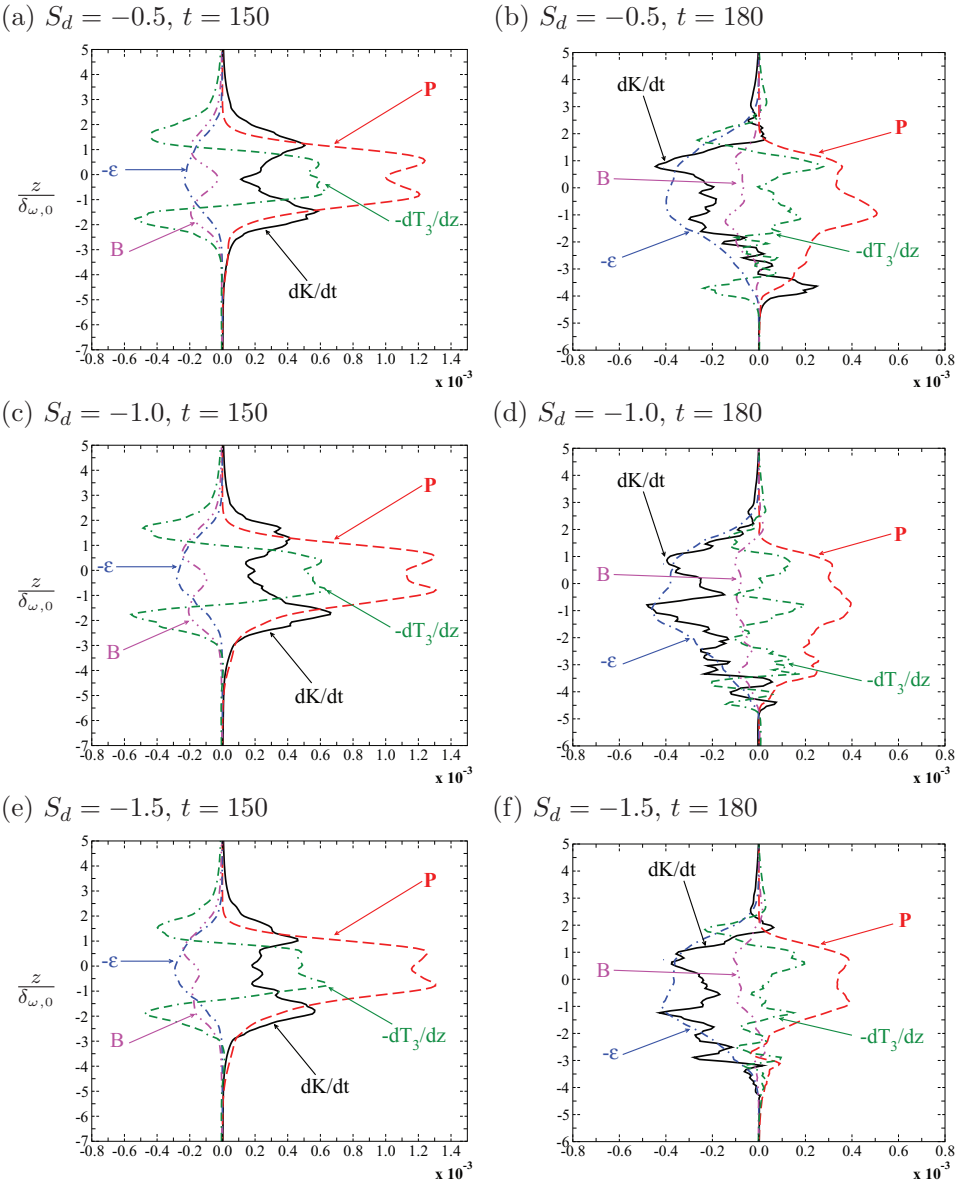

Figure 7. Turbulent kinetic energy budgets for the three cases at $t = 150$ and 180.

not wave transport (the pressure–velocity correlation). The number of bursts are different among the cases. In Case $S_d = -1.5$, the stratification is so strong that the vortices are likely to be broken down before reaching this depth. In contrast, the shear in Case $S_d = -0.5$ is so weak that not as many vortices can be ejected from the top shear layer. Case $S_d = -1.0$, with a moderate value of shear and stratification, has the largest number of bursts. The intensity of each burst also varies and reflects the strength of the penetrating vortices. With each burst in the transport, there is an accompanying burst in the production. The production burst is due to the Reynolds stress $< u'w' >$ transported down by the vortices

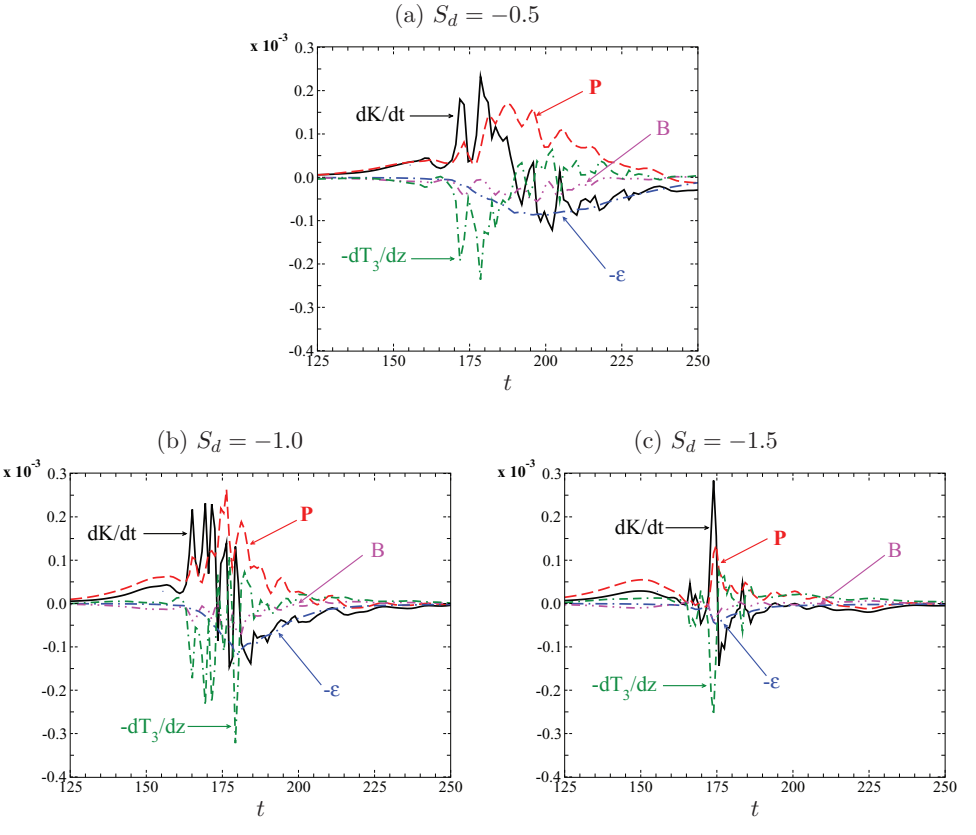

Figure 8. Turbulent kinetic energy budgets for the three cases at depth $z = -3.5$.

seeing the shear in the bottom layer. The dissipation increases after the first burst. After $t = 180$, when all the bursts have occurred, the production continues to be large at this depth. The production during this late period is due to the interaction of residual turbulent fluctuations with the existing mean shear, which is equivalent to extraction of TKE from the bottom current. For Cases $S_d = -0.5$ and -1.0, integrating the terms in the budget over time yields a net production that is larger than the energy transports, and therefore, the mean shear in the bottom current must be a source of TKE. Clearly, even though the gradient Richardson number is as large as 0.4 at this depth, as shown in Figure 5(c), TKE can still be extracted from the background flow.

In Figure 9(a)–(c), we plot the terms in the TKE budget, integrated over the region $-7 < z < -2$, for the three cases to illustrate the net effects of the vortices on the energetics of the bottom shear layer. Among the cases, the peak values of all terms are smallest in Case $S_d = -1.5$, where the strong stratification opposes the vortex penetrations. It is noted that the largest peak value of transport, which occurs in Case $S_d = -0.5$, does not trigger the largest production and dissipation. Although the peak transport value in Case $S_d = -1.0$ is smaller, the peak value of production and dissipation are larger. The larger shear in this case contributes more energy to the TKE budget. Integrating the production and transport in Figure 9(b) over the simulated time for Case $S_d = -1.0$ indicates that the net production is approximately three times larger than the net downward energy transport by the vortices.

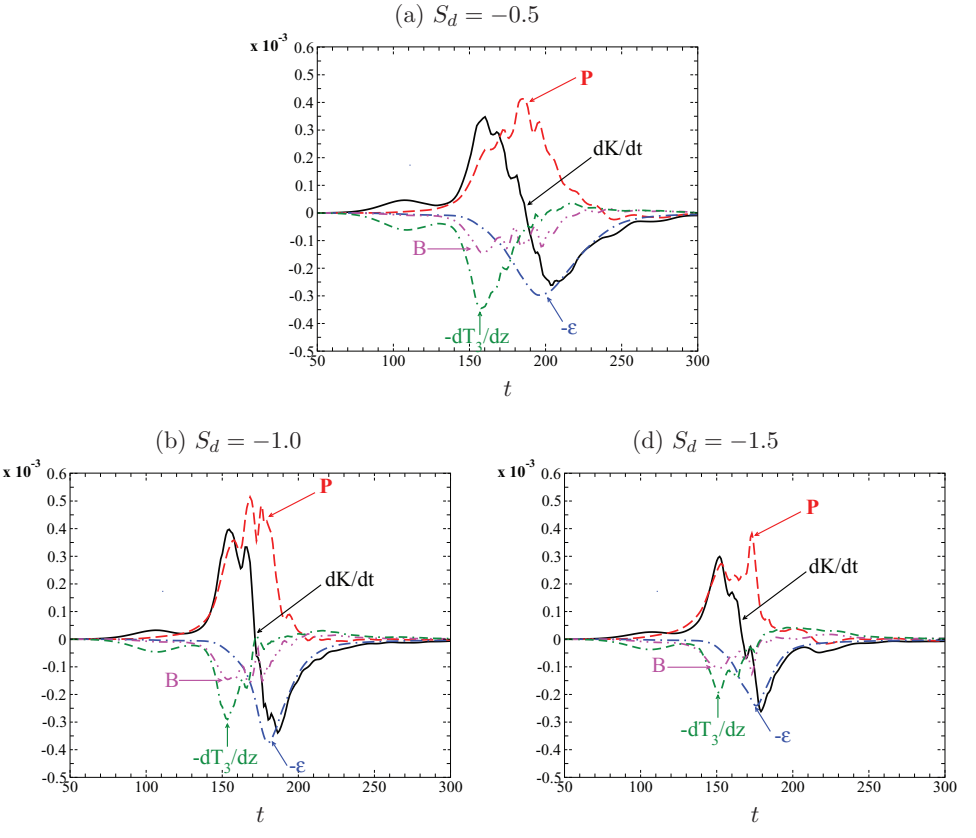

Figure 9. Integrated turbulent kinetic energy budgets for the three cases over the region $-7 < z < -2$.

While the turbulent flux of the penetrating vortices is crucial in triggering the turbulence generation, the available mean kinetic energy in the background flow is the major contributor to TKE for mixing.

6. Turbulent mixing

The intermittent patches of turbulence in the bottom shear layer are not only highly dissipative, as shown in the last section, but the mixing rate there is also intense. Figure 10(a)–(c) shows the scalar dissipation fields, χ_ρ, corresponding to the TKE dissipation fields in Figure 6. Here, χ_ρ is computed as $2Re_0^{-1}\mathrm{Pr}^{-1} < (\partial\rho'/\partial x_i)^2 >$. It is clear from the figures that the scalar dissipation inside the turbulence patches in the bottom layer is as strong as that in the shear-driven turbulence in the top layer at $t = 180$. The vortices not only carry TKE but also push light fluid downward into the strongly stratified bottom layer. The deeper the vortices impinge, the larger are the buoyancy flux and the scalar dissipation. The red patch of scalar dissipation in the region $0 < x < 10$ and $-5 < z < -2$ in Figure 10(b) is significantly larger than the size of the horseshoe vortices, so dynamics local to the region also contribute to the mixing. For example, recall that the isopycnals in Figure 2(c) in the

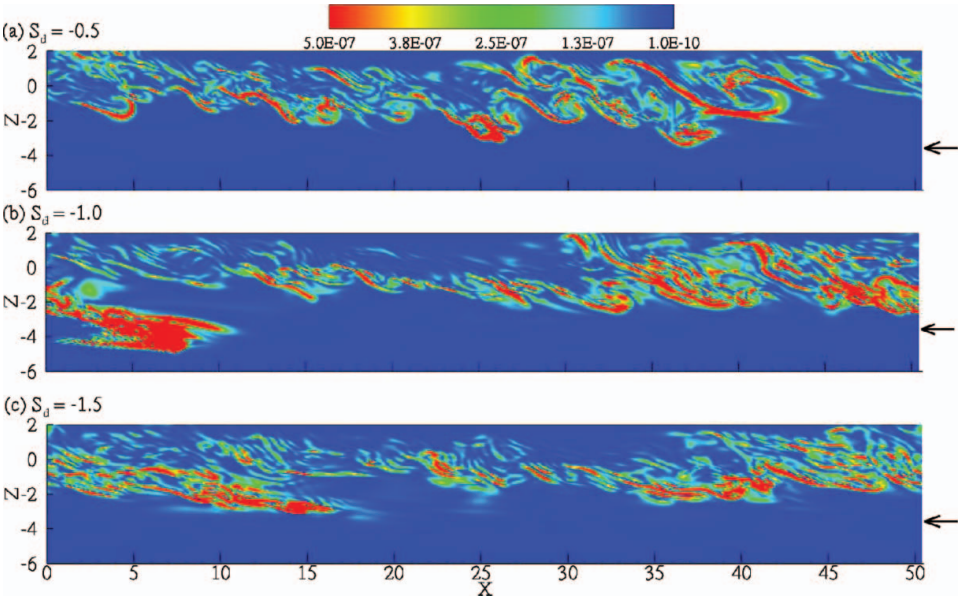

Figure 10. Scalar dissipation fields in $x - z$ slices at $y = -16.7$ in the three cases at $t = 180$. Arrows indicate the center of the bottom shear layer.

region $40 < x < 45$ in the bottom shear layer have large-amplitude displacement, so they subsequently overturn and contribute to mixing.

To compare the mixing among the cases, we plot the time evolution of the dissipation rate of the turbulent potential energy, ε_ρ, at $z = -3.5$ in Figure 11(a). This quantity is defined as $\varepsilon_\rho = \chi_\rho / N^2$. Case $S_d = -1.0$ has the largest peak value of ε_ρ, while Case $S_d = -0.5$ has the longest time period of mixing. While the peak value in the former is 25% larger, its duration is approximately 40% shorter. Integrating over time, the net potential energy dissipation in Case $S_d = -0.5$ is twice as large as that in Case $S_d = -1.0$.

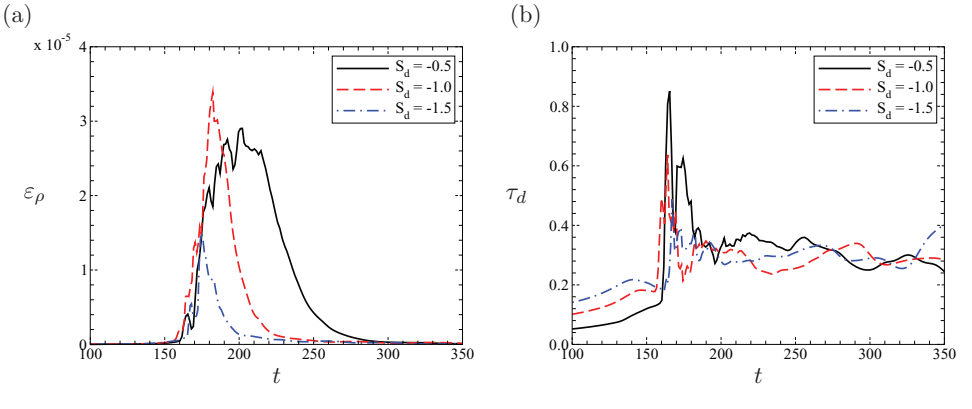

Figure 11. (a) Dissipation rate of the turbulent potential energy at depth $z = -3.5$; (b) mixing efficiency at depth $z = -3.5$.

Thus, the bottom shear layer in Case $S_d = -0.5$, with the weakest stratification, has the largest net mixing. The evolution of the TKE dissipation rate ε at $z = -3.5$ also shows that this case has the largest time-integrated TKE dissipation. With a fixed gradient Richardson number, a weak shear and a low stratification in the bottom shear layer yield the largest net dissipation in both the turbulent kinetic and potential energy budgets.

The time evolution of the mixing efficiency, $\tau_d = \varepsilon_\rho/\varepsilon$, at $z = -3.5$ is shown in Figure 11(b). As the vortices penetrate this depth, the mixing efficiency spikes to a large value. This mixing elevation due to vortex dynamics is also observed in the top shear layer when vortices associated with KH billows are formed. In Case $S_d = -0.5$, the peak value for mixing efficiency is 0.8 in the bottom layer (in Figure 11(b)) and is 2.2 (not shown) at $z = 0$ in the top layer during the roll-up of KH billows. With the size of horseshoe vortices significantly smaller than that of a KH roller, a mixing efficiency of 0.8 is significant. After the vortices break down at $t = 180$, the mixing efficiency is clustered about the value of 0.35 in all cases, which is comparable to the value of decaying turbulence in a unstable shear layer [11] as well as that of decaying turbulence generated by Taylor–Green vortices [19].

7. Conclusions

In the present study, we have used DNS to examine the evolution of turbulence patches driven by horseshoe vortices penetrating a stable shear layer with the gradient Richardson number Ri_g greater than 0.25. The horseshoe vortices are intermittently formed during the nonlinear evolution of an unstable shear layer ($Ri_g < 0.25$) located above. The background condition in the stable shear layer is varied to illustrate how the the vortices affect the dynamics of the turbulence patches. Three cases having the *same* value of Ri_g in the stable shear layer are simulated with different values of shear rate, S_d, and stratification.

In Case $S_d = -1.5$, in which both the shear and the stratification are strongest, the vortices are less likely to penetrate deep into the stable shear layer and are quickly dissipated due to the strong stratification. In Case $S_d = -1.0$, with moderate values of shear and stratification, the vortices penetrate across the stable shear layer. Localized patches of turbulence with intense dissipation rate are observed inside the layer. Lastly, in Case $S_d = -0.5$, with the weakest level of shear and stratification, the vortices not only penetrate the stable shear layer but also persist for the longest duration. The net TKE dissipation as well as the net turbulent potential energy dissipation are largest, and therefore, the net mixing is strongest in this case. Analysis of the TKE budget indicates that although the vortex penetrations trigger the generation of the turbulence patches, dynamics local to the stable shear layer contribute a larger amount of energy to turbulent mixing. The evolution of mixing efficiency is similar in all cases, with an elevation to a large value, up to 0.8, during the vortex penetration and a decrease to a value of 0.35 during the decay of the patches. The latter value is comparable to that observed during the decay stage of turbulence driven by an unstable shear layer with $Ri_g < 0.25$.

Acknowledgements

We are grateful for support provided by the NSF (National Science Foundation) OCE-0961184 (program monitor E.C. Itsweire).

References

[1] E.D. Zaron and J.N. Moum, *A new look at Richardson number mixing schemes for equatorial ocean modeling*, J. Phys. Oceanogr. 39 (2009), pp. 2652–2664.

[2] H.T. Pham and S. Sarkar, *Internal waves and turbulence in a stable stratified jet*, J. Fluid Mech. 648 (2010), pp. 297–324.
[3] P. Hazel, *Numerical studies of the stability of inviscid stratified shear flows*, J. Fluid Mech. 51 (1972), pp. 39–61.
[4] J. Moum, D. Hebert, C. Paulson, and D. Caldwell, *Turbulence and internal waves at the equator. Part I: Statistics from towed thermistors and a microstructure profiler*, J. Phys. Oceanogr. 22 (1992), pp. 1330–1345.
[5] R.C. Lien, E. D'Asaro, and M. McPhaden, *Internal waves and turbulence in the upper central equatorial Pacific: Lagrangian and Eularian observations*, J. Phys. Oceanogr. 32 (2002), pp. 2619–2639.
[6] E.J. Strang and H.J.S. Fernando, *Entrainment and mixing in stratified shear flows*, J. Fluid Mech. 428 (2001), pp. 349–386.
[7] S.A. Thorpe, *Experiments on instability and turbulence in a stratified shear flow*, J. Fluid Mech. 61 (1973), pp. 731–751.
[8] C.G. Koop and F.K. Browand, *Instability and turbulence in a stratified fluid with shear*, J. Fluid Mech. 93 (1979), pp. 135–159.
[9] C. Staquet and J.J. Riley, *A numerical study of a stably-stratified mixing layer*, in *Turbulent Shear Flows 6*, Berlin, 1989, pp. 381–397.
[10] W.D. Smyth and J.N. Moum, *Length scales of turbulence in stably stratified mixing layers*, Phys. Fluids 12 (2000), pp. 1327–1342.
[11] W.D. Smyth, J.N. Moum, and D.R. Caldwell, *The efficiency of mixing in turbulent patches: Inferences from direct simulations and microstructure observations*, J. Phys. Oceanogr. 31 (2001), pp. 1969–1992.
[12] C.P. Caulfield and W.R. Peltier, *The anatomy of the mixing transition in homogeneous and stratified free shear layers*, J. Fluid Mech. 413 (2000), pp. 1–47.
[13] S. Basak and S. Sarkar, *Dynamics of a stratified shear layer with horizontal shear*, J. Fluid Mech. 568 (2006), pp. 19–54.
[14] K.A. Brucker and S. Sarkar, *Evolution of an initially turbulent stratified shear layer*, Phys. Fluids 19 (2007), 101105.
[15] C. Staquet, *Mixing in a stably stratified shear layer: Two- and three-dimensional numerical experiments.*, Fluid. Dyn. Res. 27 (2000), pp. 367–404.
[16] W.D. Smyth, and J.N. Moum, *Anisotropy of turbulence in stably stratified mixing layers*, Phys. Fluids 12 (2000), pp. 1343–1362.
[17] J. Jeong and F. Hussain, *On the identification of a vortex*, J. Fluid Mech. 285 (1995), pp. 64–94.
[18] H.T. Pham, S. Sarkar, and K.A. Brucker, *Dynamics of a stratified shear layer above a region of uniform stratification*, J. Fluid Mech. 630 (2009), pp. 191–223.
[19] J.J. Riley and S.M. deBruyn Kops, *Dynamics of turbulence strongly influenced by buoyancy*, Phys. Fluids 15 (2003), pp. 2047–2059.